Proceedings of ASME Turbo Expo 2011
GT2011
June 6-10, 2011, Vancouver, British Columbia, Canada

GT2011-46199

WATER TANK EXPERIMENTAL TESTING OF A DRAG-DRIVEN VARIABLE-BLADE GEOMETRY VAWT

Marco Raciti Castelli (*), **Igor Zotti** (**), **Ernesto Benini** (*)

(*) Department of Mechanical Engineering – University of Padova
Via Venezia, 1 – 35131 Padova, Italy
marco.raciticastelli@unipd.it, ernesto.benini@unipd.it

(**) Department of Naval Architecture, Ocean and Environmental Engineering
Via A. Valerio, 10 – 34127 Trieste, Italy
zotti@units.it

ABSTRACT

This paper presents a mean for contrasting the counter-rotating (parasitic) torque generated from drag-driven vertical-axis wind turbine (VAWT) blades travelling into the wind through the use of a variable rotor blade geometry. Water tank experimental tests of energy performance on a small rotor characterized by three horizontal blades having variable geometry were conducted. Each blade was obtained by connecting a horizontal flat plate to a tilting one swinging over a horizontal axis, so that the tilt angle between the two plates could vary depending on flow field conditions.

The results of experimental tests are proposed on the bases of two different blade profile architectures: first experimental investigations were performed on a fixed-angle blade configuration by analyzing the efficiency of different angles between the two plates. Then, attention mainly focused on tilting blades, achieving a quantification of the influence of blade swinging on overall rotor performance.

A preliminary campaign of analysis was completed for both blade configurations and overall rotor torque and power were analyzed as a function of incoming relative flow velocity and rotor angular speed, resulting the variable-blade configuration maximum power coefficients from 5 to 10 times higher with respect to the corresponding classical drag-type fixed-blade architecture.

NOMENCLATURE

A [m^2]	rotor swept area
c [mm]	blade chord length
C_p [-]	rotor power coefficient
C_T [-]	rotor instantaneous torque coefficient
D_{ext} [mm]	torque meter shaft external diameter
D_{int} [mm]	torque meter shaft internal diameter
D_{rotor} [mm]	rotor diameter
Δ D_{rotor} [mm]	estimated uncertainty in rotor diameter measurement
E [N/mm^2]	steel modulus of elasticity
g [m/s^2]	standard gravitational acceleration (assumed 9.806 in accordance to the 3rd CGPM, 1970)
GF [-]	gage factor
H_{rotor} [mm]	rotor height
Δ H_{rotor} [mm]	estimated uncertainty in rotor height measurement
H_{wt} [m]	water tank depth
L [m]	water tank total length
L_a [mm]	lever arm for torque meter calibration
N_g [-]	number of active gages (4 for torque measurements)
N [-]	number of blades
P [W]	rotor power
R [-]	ratio between rotor swept area and water tank test section
R [mm]	rotor radius
Re [-]	blade chord based Reynolds number
Res [Nm]	torque meter resolution
s [mm]	blade plate thickness

S_{trans} [mV/m]	transmitter sensitivity
T [Nm]	rotor torque
$T_{full\ scale}$ [Nm]	full scale torque range of the measurement system
ΔT [Nm]	estimated uncertainty in rotor torque measurement
$V_{test\ section}$ [m/s]	mean relative water velocity at rotor test section
V_∞ [m/s]	relative water velocity
$\Delta V_\infty^3\%$ [-]	percentage increase in the cube of the relative velocity at rotor test section
ΔV_∞ [m/s]	estimated uncertainty in relative water velocity measurement
ΔV_{torque} [-]	torque meter output signal
W_{wt} [m]	water tank section width
β [°]	maximum tilt angle with respect to horizontal blade element
ε_{sb} [-]	solid blockage correction factor
μ [Pa·s]	water viscosity at 20°C (assumed $1.002 \cdot 10^{-3}$)
ρ [kg/m^3]	water density (assumed 1000)
Δρ [kg/m^3]	estimated uncertainty in water density measurement
υ [-]	Poisson's ratio
ω [rad/s]	rotor angular velocity
Δω [rad/s]	estimated uncertainty in rotor angular velocity measurement

INTRODUCTION AND BACKGROUND

One of the key performance differences in wind turbine design is determined by the driving mechanism of the rotor. As focused by Gipe [1], drag devices are quite simple wind machines which use flat or cup-shaped blades to turn a rotor around a vertical axis. In these configurations, the wind merely pushes on the blade, forcing it to move downwind and making the rotor spin about its vertical axis. Though researchers constantly propose innovative solutions in order to use drag to power wind turbines, drag propulsion appears be affected by intrinsic physical limitations, especially if compared to more efficient lift-driven devices. The differences between the two rotor concepts are in fact quite relevant:

- drag-driven wind turbines typically combine a low aerodynamic efficiency with a high blade surface requirement and, consequently, are usually rather expensive to be manufactured when set against their comparatively limited power output;
- lift-driven wind turbines combine a high aerodynamic efficiency, nearly up to the theoretical Betz limit, with a much more favourable blade surface requirement.

While small scale lift-driven VAWTs have already reached a good level of commercial awareness, drag type devices seem to be limited to prototype stage, mainly used for water pumping or some other direct mechanical applications, being considered not suitable for electricity generation, due to a too low value of the tip speed ratio parameter and, consequently, a comparatively lower power coefficient [2]. Nevertheless, as pointed out by Manwell et al. [3], the main argument in favour of drag-driven machines is the relatively low construction cost, which makes them less expensive than comparable lift-driven devices, thus allowing an initial saving in a micro wind project economics. Therefore, several authors concentrated on drag-driven VAWTs, especially on Savonius rotors, in order to improve their efficiency.

Menet and Bourabaa [4] improved the aerodynamic characteristics of a Savonius rotor by identifying the most aerodynamically salient geometric parameters and proposing a new machine architecture based on their optimization. The effect of some aerodynamic devices, such as a central shaft and an external chassy, was also studied with the aim of further improving rotor performance.

Altan and Atilgan [5] studied a mechanical device in order to increase the low performance of a Savonius rotor by placing a special curtain in front of the rotor with the aim of preventing the counter-rotating torque that occurs on the convex blade while spinning in the negative direction. Both experimental measurements and numerical analysis were conducted and the positive effect of the curtain on overall machine performance was proved.

Nakajima et al. [6] performed water tank experiments in order to investigate the influence of a 90° phase shift angle between a two-staged laid-upon Savonius blades on overall rotor performance, obtaining a maximum increase of 10% in the measured power coefficient, compared with the original single-step configuration.

Saha and Rajkumar [7] explored the feasibility of twisted bladed Savonius rotor for power generation through low speed wind tunnel measurements in comparison with conventional semicircular blades, characterized by a twist angle of 0°. Performance analysis was conducted on the basis of starting characteristics, static torque and rotational speed, demonstrating the potential of the twisted bladed rotor in terms of smooth running, higher efficiency and self-starting capability.

Another advantage of drag-driven machines is their excellent self-starting capabilities, even for very low wind speeds, in contrast to lift-driven devices, which require external assistance to start, thus loosing much of their aerodynamic advantage, especially in sites characterized by variable winds, as suggested by Dominy et al. [8].

In order to combine lift-driven turbines high performance and drag-driven devices self-starting capabilities, Gupta et al. [9] performed experimental investigations of a combined Savonius-Darrieus VAWT, obtaining an increase in overall rotor power coefficient for low values of tip speed ratio and a decrease in rotor power coefficient for high values of tip speed ratio.

The main drag-driven devices disadvantage is due to the constant presence of at least one blade travelling into the wind, thus creating additional drag on the machine as it spins. As discussed before, Altan and Atilgan [5] tried to overcome this problem by placing a mechanical obstacle to wind in front of rotor blades while spinning in the negative direction. Nevertheless, this solution presents the disadvantage of requiring the continuous orientation of the obstacle, thus loosing much of the aerodynamic advantage of VAWTs, that is their independence from wind direction, which is of primary importance for micro wind turbines operating in gusty wind conditions.

In the present work the counter-rotating torque generated by the blade travelling into the wind is contrasted by using variable rotor blade geometry, allowing the counter-rotating blade to collapse into a simple flat plate during its passive period of revolution, thus reducing the negative contribution to torque, as can be seen in Figure 1.

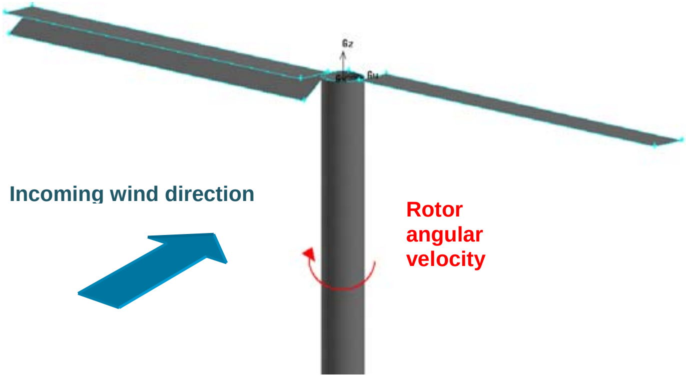

Figure 1: Exemplification of blade full opening during active period of revolution (left) and collapsing during passive (counter-rotating) period of revolution

A preliminary campaign of analysis was completed for both fixed and tilting blade configurations: overall rotor torque and power were analyzed as a function of incoming flow velocity and rotor angular speed, achieving a first quantification of the influence of blade swinging on overall rotor performance.

MODEL GEOMETRY

Figure 2 shows a view of the tested rotor, which basically consisted in three horizontal flat blades spinning around a vertical axis. As can be seen, a flat wing-tip device was positioned at the end of each blade in order to reduce negative effects due to finite blade span extension. A small vertical reinforcement was positioned at blade mid-span in order to increase total blade stiffness. The model was constructed from aluminium mounted on a 100 mm diameter steel rod. Table 1 summarizes the main features of the rotor.

Denomination	Value
Rotor radius, R [mm]	500
Blade chord length, c [mm]	120
Blade plate thickness, s [mm]	3
Blade number, N [-]	3

Table 1: Main features of the tested rotor

As can be seen in Figure 3, each blade is composed of two flat plates:

- an upper blade element, fixed and horizontal;
- a lower blade element, free of tilting around the leading edge up to a pre-determined inclination angle with respect to the horizontal, depending on flow field conditions.

In order to perform a comparison between tilting blade configuration and conventional fixed-blade geometry, a special mechanical gauge block allowed locking the lower blade element in a pre-determined inclination angle with respect to the horizontal.

Figure 2: View of the tested rotor; open and fixed blade configuration

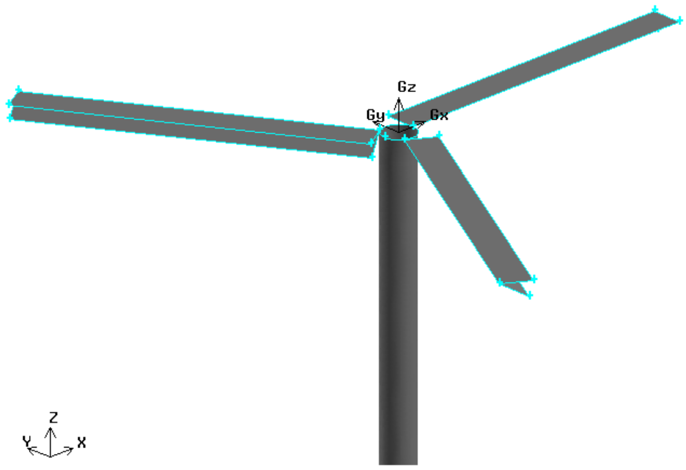

Figure 3: 3D-model of the tested rotor; 31.6° open and fixed blade configuration

Denomination	Maximum tilt angle with respect to horizontal blade element, β [°]
Model 19.5	19.5
Model 31.6	31.6
Model 41.8	41.8
Model 59.0	59.0

Table 2: Maximum tilt angle with respect to the horizontal blade element for the four tested rotor configurations

Table 2 summarizes the maximum tilt angle with respect to the horizontal blade element for the four tested rotor configurations, which were respectively named, after their maximum lower blade element tilt angle with respect to the horizontal, as *Model 19.5*, *Model 31.6*, *Model 41.8* and *Model 59.0*.

Table 3 summarizes the resultant rotor heights and swept areas for the four analyzed rotor configurations.

Denomination	Rotor height, H_{rotor} [mm]	Rotor swept area, A [m^2]
Model 19.5	35.0	0.035
Model 31.6	55.0	0.055
Model 41.8	70.0	0.070
Model 59.0	90.0	0.090

Table 3: Resultant rotor heights and swept area for the four analyzed rotor configurations

TEST FACILITY AND EXPERIMENTAL APPARATUS

Experimental tests were carried out at the Department of Naval Architecture, Ocean and Environmental Engineering water tank in Trieste, Italy, shown in Figure 4. The facility is equipped with a towing carriage running on two rails on either side, equipped with a speed control system and capable of towing the model, thus generating a relative velocity between the rotor and the water. For the adopted test model configuration, a maximum free-stream relative velocity of 2.1 m/s was available. The relative Reynolds number, based on blade chord, was therefore (being the tested device a drag-type rotor, operating at TSR values lower than 1, the Reynolds number was calculated with respect to the free-stream relative velocity):

$$Re = \frac{\rho V_\infty c}{\mu} = 252000 \quad (1)$$

corresponding to a 2.5 m diameter and 300 mm blade chord rotor operating in air for an unperturbed wind velocity of 12.5 m/s (being air density assumed 1.25 kg/m^3).

Figure 4: View of the Department of Naval Architecture, Ocean and Environmental Engineering water tank, Trieste, Italy

Table 4 summarizes the water tank main geometrical features.

Denomination	Dimension [m]
Water tank total length, L	45
Water tank section width, W_{wt}	3.0
Water tank depth, H_{wt}	1.5

Table 4: Water tank main geometrical features

The ratio between the rotor swept area for the maximum lower blade element inclination angle (for *Model 59.0* rotor configuration) and the water tank test section can be obtained as:

$$R = \frac{A}{W_{wt} \cdot H_{wt}} = 0.03 \quad (2)$$

Being the geometric blockage of the model in the water tank rather small, no interference corrections were considered: the value of solid blockage correction factor and its relative velocity correction at rotor test section were calculated according to [10], in formulas:

$$\varepsilon_{sb} = 1/4 \frac{D_{rotor} \cdot H_{rotor}}{W_{wt} \cdot H_{wt}} \quad (3)$$

$$V_{test\ section} = (1 + \varepsilon_{sb}) V_\infty \quad (4)$$

Table 5 reports the calculated values of solid blockage and percentage increase in the cube of the relative velocity at rotor test section, defined as:

$$\Delta V_\infty^3 \% = 100 \cdot \frac{V_{test\ section}^3 - V_\infty^3}{V_\infty^3} \quad (5)$$

for the four analyzed rotor configurations. As can be seen, the maximum increase (for *Model 59.0* rotor configuration) in the cube of the relative velocity at rotor test section, with respect to the value of unperturbed relative water velocity in front of the rotor itself, resulted of 1.51%. Since the estimation of the correct value of wake blockage was rather difficult, and being the overall experimental domain over-sized by imposing the requirement on the cube of the relative velocity at the test section, the wake blockage was not considered in the calculation of rotor power coefficient.

Denomination	ε_{sb} [-]	ΔV^3 [%]
Model 19.5	0.0019	0.58
Model 31.6	0.0030	0.92
Model 41.8	0.0039	1.17
Model 59.0	0.0050	1.51

Table 5: Calculated values of solid blockage and increase in the cube of the velocity at rotor test section for the four analyzed rotor configurations

A schematic view of the test model instrumentation and measurement system is shown in Figure 5. The rotor was hooked downward to the towing carriage on the top of the water basin, being one end of the shaft coupled to an upper mounted torque meter. The rotor was positioned at the geometrical centre of the test section, resulting 0.75 m far away from both the freesurface and the water tank floor. Being the total height of the rotor quite small (presenting a maximum value of 0.09 m for *Mod 59.0* configuration) the influence of the boundary conditions on overall rotor performance was considered negligible. Being however the ratio of rotor diameter to water tank width relatively high, as can be determined by the following relation:

$$R = D/W_{wt} = 0.33 \qquad (6)$$

there was some concern about the possible influence of the lateral water tank walls on overall rotor performance. Some CFD simulations should be performed in order to precisely quantify the phenomenon.

The rotor was kept at a constant angular velocity by means of a DC motor supplied by four batteries and controlled by a service model for the maintenance of a desired rotating speed. Transmission between rotor and electrical motor was held by a pulley, allowing a reduction of motor angular velocity of 5:1.

Measurements were conducted using a single-channel, non-contact, inductively-powered Binsfeld Engineering Torque Track Revolution torque meter. The system, consisting in an aluminium rotating shaft collar with integral transmitter module and a master control unit with a stationary power ring, provided continuous torque, angular velocity and power to an external acquisition system. Data were sampled at 1000 Hz.

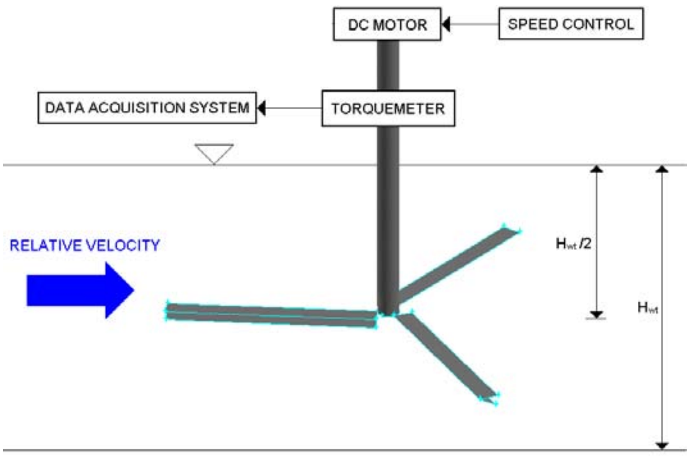

Figure 5: Schematic view of the test model instrumentation and measurement system

Figure 6 shows the operating rotor hooked downward to the towing carriage on the top of the water basin, while Figures 7 and 8 present respectively a 3D-modelling and an upper view of the transmission system and of the assembly between the torque meter and the relative supporting frame.

Figure 6: View of the tested rotor hooked downward to the towing carriage on the top of the water basin

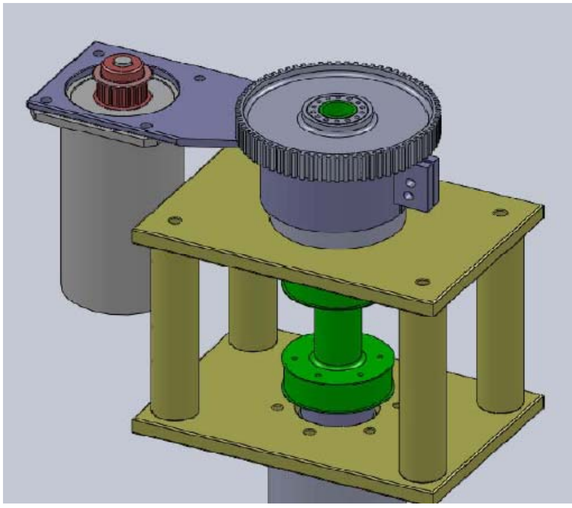

Figure 7: 3D-modelling of the transmission system and of the assembly between the torque meter (green) and the relative supporting frame (brown)

Figure 8: Upper view of the transmission system; DC motor and rotor axis were connected through a rubber timing belt

Figures 9 and 10 show a view of the torque meter shaft with the strain gages and a schematic description of the fixed and rotating sub-systems. The angular velocity signal was generated by six magnets, placed inside the rotating collar, which triggered the pickup sensor at the base of the power ring.

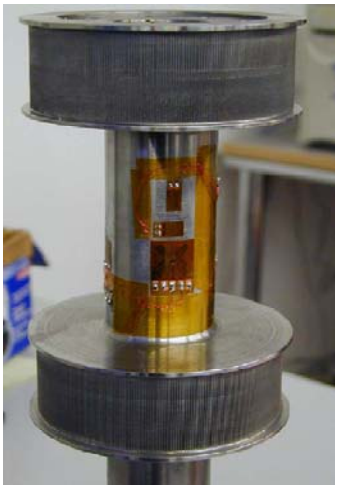

Figure 9: Torque meter shaft with strain gages

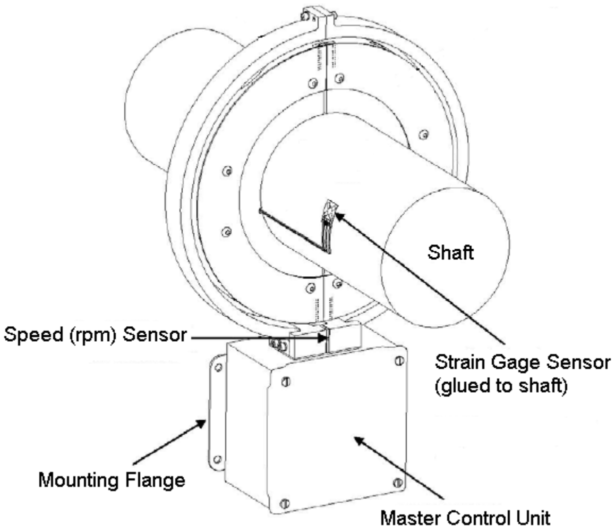

Figure 10: Schematic description of torque meter fixed and rotating sub-systems

Table 6 summarizes the torque meter main geometrical and functional features.

Denomination	Value
S_{Trans}	1 mV/m
GF	2.045
E	$69 \cdot 10^3$ N/mm^2
υ	0.33
D_{ext}	47 mm
D_{int}	44 mm

Table 6: Torque meter main geometrical and functional features

The full scale torque range of the system, based on shaft parameters, strain gage parameters and the transmitter gain setting, was defined by the following general relation [11]:

$$T_{\text{Full scale}} = \frac{4 S_{\text{Trans}} \pi E (D_{\text{ext}}^4 - D_{\text{int}}^4)}{16 \cdot 10^6 GF \cdot N_g (1+\nu) D_{\text{ext}}} = 119.9 \text{ Nm} \quad (7)$$

Being overall system resolution of 14 bits, torque meter resolution was determined from the following relation:

$$\text{Res} = \frac{2 T_{\text{Full scale}}}{2^{14}} = 0.014 \text{ Nm} \quad (8)$$

Figure 11: Assembled test-bench. The special frame, composed by two aluminium plates connected with four aluminium columns, is visible

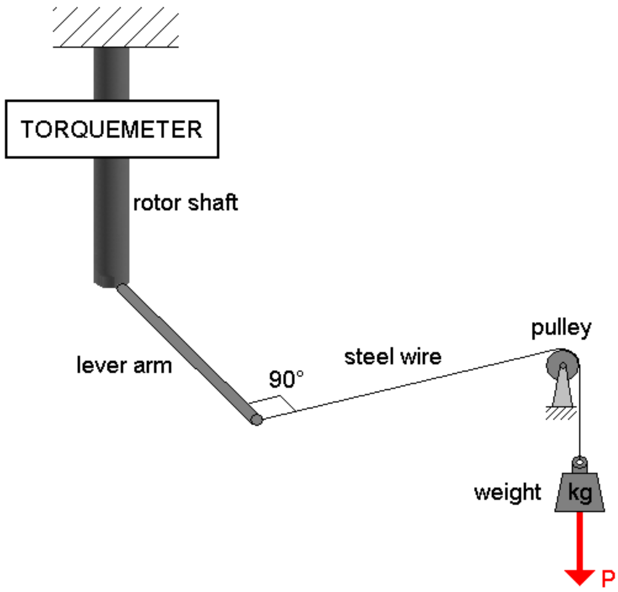

Figure 12: Schematic description of the torque meter calibration procedure

In order to prevent the torque meter substaining structure from bending, a special frame composed by two aluminium plates measuring 250 x 360 x 20 mm and connected with four auminium columns was manifactured. The aluminium plates were CNC machined so as to guarantee an accurate alignment between the central holes and the parallelism between their upper and lower surfaces, as can be seen in Figure 8. Figure 13 shows a picture of the assembled test-bench.

Torque meter calibration was performed under steady and controlled conditions, just before starting the experimental measurements, in order to avoid every source of uncertainties due to local temperature and relative humidity. The vertical shaft of the rotor was loaded by different torque values by means of horizontal forces applied to the end of a stainless steel lever arm. Each horizontal force was obtained through a system made of a weight connected to the lever arm by a steel wire and a pulley, as explained in Figure 12.

Table 7 summarizes the weight values and the relative uncertainties adopted for torque meter calibration. The adopted lever arm measured 10.4 ± 0.1 mm.

m [kg]	Δm [kg]
0.350	± 0.003
0.707	± 0.003
1.079	± 0.003
2.158	± 0.003
5.020	± 0.003
7.178	± 0.003
10.060	± 0.003
12.218	± 0.003
15.130	± 0.003

Table 7: Weight values and relative uncertainties adopted for torque meter calibration

Figure 13 represents the torque meter characteristic curve, determined through linear regression. Being the applied torque determined by the relation:

$$T = L_a m\, g \quad (9)$$

torque error bars were calculated for each measured calibration point through the uncertainty propagation criterion based on partial derivatives, in formulas:

$$\Delta T = \sqrt{\left(\frac{\partial T}{\partial L_a}\Delta L_a\right)^2 + \left(\frac{\partial T}{\partial m}\Delta m\right)^2} \quad (10)$$

In order to determine the uncertainty on experimentally measured torque values, two straight lines were then traced, parallel to the regression line, so as to include all calculated error bars, as shown in Figure 13. The correspondent uncertainty for torque measurements resulted ΔT = ± 0.6 Nm.

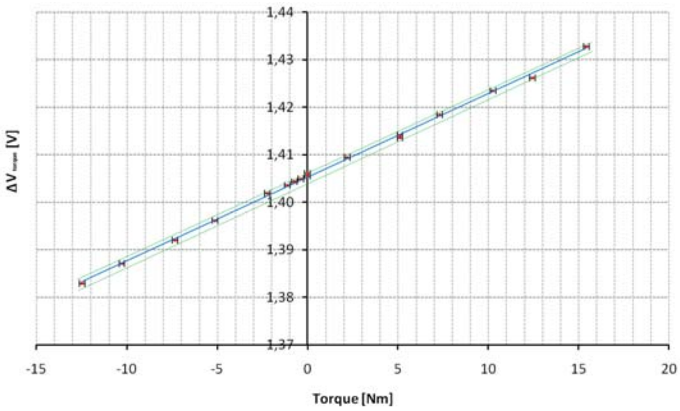

Figure 13: Torque meter characteristic curve, relative error bars and straight lines, traced parallel to the regression line, in order to determine the uncertainty on experimentally measured torque values

TEST RESULTS AND DISCUSSION

All the measurements presented in this work were performed for a relative velocity of 2.1 m/s between rotor and water. For each measurement, in order not to take into account the acceleration phase of the towing carriage, data acquisition started only when a constant relative speed was reached.

The results of experimental tests are proposed on the bases of two different blade profile architectures: first experimental investigations were performed on a fixed-angle blade configuration, comparing the performance of different angles between the lower rotor blade element and the orizontal plane. Then the attention mainly focused on tilting blades, allowing a performance comparison between the conventional fixed drag-driven configuration and the proposed variable configuration.

Figures 14 and 15 represent the evolution of the power coefficient, defined as:

$$C_P = \frac{P}{0.5 \rho A V_\infty^3} \quad (11)$$

for all of the tested rotor configurations as a function of the tip speed ratio, defined as:

$$TSR = \frac{\omega R}{V_\infty} \quad (12)$$

Table 8 summarizes the uncertainties adopted for the calculation of error bars in Figures from 14 to 16.

Once more, torque error bars were calculated through the uncertainty propagation criterion based on partial derivatives, in formulas:

$$\Delta C_p = \sqrt{\sum_{i=1}^{n}\left(\frac{\partial C_p}{\partial x_i}\Delta x_i\right)^2} \quad (13)$$

being:

$$\frac{\partial C_p}{\partial T} = \frac{\omega}{0.5\rho D_{rotor} H_{rotor} V_\infty^3} \quad (14)$$

$$\frac{\partial C_p}{\partial \omega} = \frac{T}{0.5\rho D_{rotor} H_{rotor} V_\infty^3} \quad (15)$$

$$\frac{\partial C_p}{\partial \rho} = -\frac{T\omega}{0.5\rho^2 D_{rotor} H_{rotor} V_\infty^3} \quad (16)$$

$$\frac{\partial C_p}{\partial D_{rotor}} = -\frac{T\omega}{0.5\rho D_{rotor}^2 H_{rotor} V_\infty^3} \quad (17)$$

$$\frac{\partial C_p}{\partial H_{rotor}} = -\frac{T\omega}{0.5\rho D_{rotor} H_{rotor}^2 V_\infty^3} \quad (18)$$

$$\frac{\partial C_p}{\partial V_\infty} = -\frac{T\omega}{0.5\rho D_{rotor} H_{rotor} V_\infty^4} \quad (19)$$

Denomination	Value
ΔT	± 0.6 Nm
$\Delta\omega$	± 0.001 rad /s
ΔV	± 0.01 m/s
$\Delta\rho$	± 0.001 kg/m^3
ΔD_{rotor}	± 0.0001 m
ΔH_{rotor}	± 0.0001 m

Table 8: Main variables uncertainties adopted for the calculation of error bars in Figures from 14 to 16

The following remarks can be drawn:

- the proposed rotor total efficiency is quite low, both for fixed and for variable-blade configurations, being the maximum power coefficient achieved by variable-blade *Model 19.5* rotor configuration approximately 6%. This was due to the fact that the tested blade geometry is not jet optimized, being the major objective of the present work to verify just the concept of tilting rotor blade energy conversion systems;
- all the measurements reported in the present work were performed for a constant relative velocity of 2.1 m/s between rotor and water. Therefore, as the Reynolds number for a drag-driven VAWT is determined with respect to the free-stream velocity, the described analysys were performed for only one value of Reynolds number. Once more, since a preliminary campaign of analysis had been presented, the influence of Reynolds number on rotor performance was not analyzed. Nevertheless, such sort of considerations should be performed in an advanced test phase;
- the maximum C_p for tilting rotor blade configuration occurred for higher TSR values with respect to the corresponding fixed-bladed configuration. This phenomenon is due to the reduced flow blockage generated by the tilting rotor blade configuration compared to the fixed one and is responsible for the general increase in rotational speed of the variable-blade architecture;
- tilting rotor blades performed quite well if compared to conventional fixed-blade architecture, being variable-blade rotor configuration maximum power coefficients from 5 to 10 times higher with respect to the corresponding fixed-blade configurations, as can be seen also from Figure 16, showing a comparison between maximum power coefficients as a function of the maximum tilt angle with respect to the horizontal blade element;
- because of electric motor limitations very low values of TSR could not be reached, thus limiting the analysis to an operational range of angular velocities where the values of C_p where not optimized. Further measurements should be performed in order to explore also the lower range of TSR values, by adding a mechanical gearbox to the transmission system, in order to improve the capability of the system to operate at very low angular velocities;
- in some cases (*Model 31.6* fixed-blade rotor configuration, *Model 41.8* and *Model 59.0* variable-blade rotor configuration) different results were obtained for the same very similar TSR values. This phenomenon is probably due to a wrong estimation of the rotor mean angular velocity due to fluctuations in the electric motor instantaneous rotational speed caused by the excessively low angular velocity range. Also this problem should be overcome by the addition of a mechanical gearbox to the transmission system. The addition of an encoder to the main rotor shaft could also improve the accuracy of the istantaneous rotational speed measurement, allowing to more precisely investigate even a very low range of angular velocities;

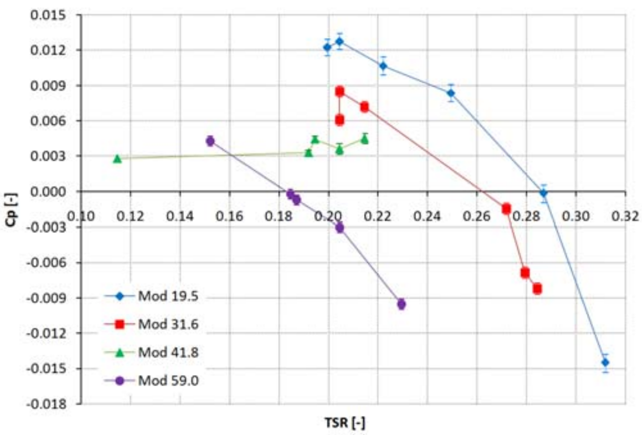

Figure 14: Evolution of the power coefficient for fixed-blade rotor configuration

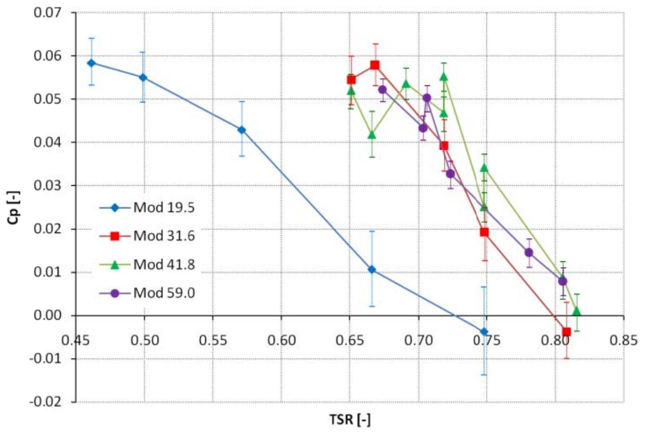

Figure 15: Evolution of the power coefficient for variable-blade rotor configuration

As can be seen from Figure 16, low values of maximum tilt angle with respect to horizontal blade element (both fixed and variable) configurations performed sligthly better than corresponing higher tilt angles. It can be argued that a low value of the β angle could allow the fluid to better step in between the two blades, thus generating more thrust, anyway the causes of this phenomenon are not yet clear and further research is to be done. Also the effect of the endplate at blade tip should be investigated, being probably connected with the outflow from the rotor blade during the active period of revolution.

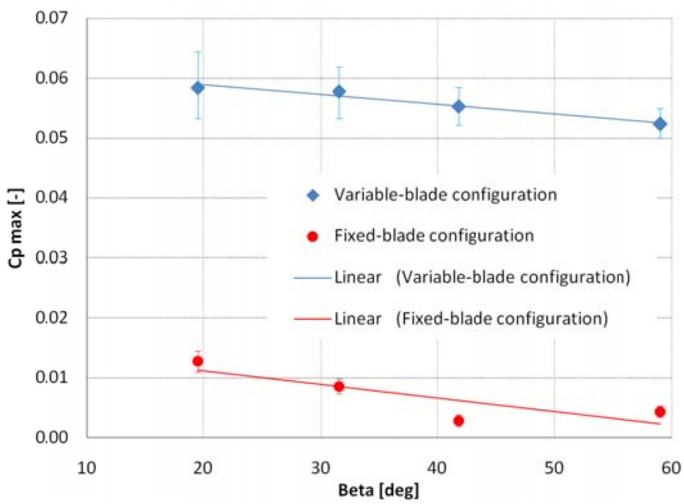

Figure 16: Comparison between fixed and variable-blade rotor configuration maximum power coefficients as a function of the maximum tilt angle with respect to horizontal blade element

Figures 17 and 18 show the evolution of the instantaneous torque coefficient, defined as:

(20)

as a function of time for both fixed and variable-blade *Model 59.0* rotor configuration. As can be seen, the sudden opening of the tilting blade in the variable-blade configuration is responsible for a relavant torque peak which is not registered for fixed-blade configuration. Having tested a three-bladed turbine, a 120° periodicity in rotor dynamic characteristic may also be noticed.

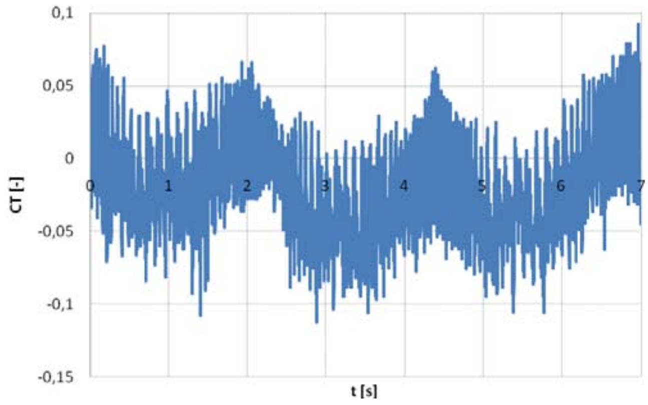

Figure 17: Evolution of the istantaneous torque coefficient as a function of time for fixed-blade *Model 59.0* rotor configuration (for the sake of clarity, just nominal torque coefficient values are shown); TSR = 0.204

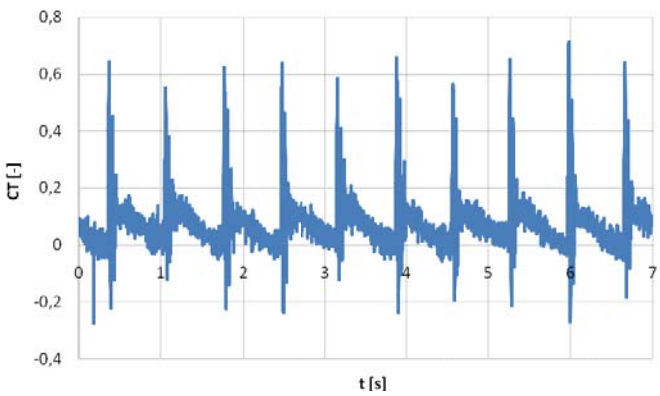

Figure 18: Evolution of the istantaneous torque coefficient as a function of time for variable-blade *Model 59.0* rotor configuration (for the sake of clarity, just nominal torque coefficient values are shown); TSR = 0.706

CONCLUSIONS AND FUTURE WORKS

A mean for furthering conventional drag-driven VAWT technology by contrasting the counter-rotating (parasitic) torque generated from blades travelling into the wind was proposed.

Through the use of a water tank for experimental testing of energy performance on a small turbine characterized by three horizontal blades, a preliminary campaign of analysis was completed for both a fixed and a tilting blade configuration, allowing the counter-rotating blade to collapse into a simple flat plate during its passive period of revolution, thus reducing the negative contribution to torque.

The prototype provided a means for testing various operating and design parameters affecting the turbine performance. Even though, due to electric motor limitations, the range of tip speed ratio conditions appears to have missed the maximum C_p values, a first quantification of the influence of blade swinging on overall rotor performance was achieved, resulting the variable-blade configuration maximum power coefficients from 5 to 10 times higher with respect to the corresponding classical drag-type fixed-blade configurations. Further measurements should be performed in order to expolre also the lower range of TSR values, by adding a mechanical gearbox to the transmission system. An encoder should also be added to the measurement system, in order to more precisely determine low values of angular velocities.

Further work on tilting blade design and blade tip endplate geometry is also to be performed in order to aerodynamically optimize the tested geometry, thus enhancing energy estraction and enabling a performance comparison between the proposed rotor architecture and conventional drag-type VAWTs. Some considerations on the influence of the Reynolds number on overall rotor performance should also be performed, by conducting several tests at different free-stream relative velocities between rotor and water.

The adoption of low values of maximum tilt angle between upper and lower blade elements (both for fixed and variable configurations) resulted in a slightly increased performance with respect to the adoption of higher tilt angles. Once again, further research is to be done in order to better investigate this phenomenon.

Finally, possible influence of the lateral water tank walls on overall rotor performance should be further investigated through CFD calculations, in order to correct any disturbance derived from the experimental boundary conditions to overall rotor performance.

ACKNOWLEDGEMENTS

The variable rotor blade geometry proposed in the present work was manufactured in accordance to the Italian Patent N. RM2009A000326 [12].

REFERENCES

[1] Gipe, P., *Wind Power – Renewable Energy for Home, farm and Business*, Chelsea Green Publishing Company, First printing: march 2004, p. 93;

[2] Hau E., *Wind Turbines – Fundamentals, Technologies, Application, Economics*, 2nd Edition, Springer-Verlag Berlin Heidelberg 2006, p. 71;

[3] Manwell, J. F., McGowan J. G., Rogers A. L., *Wind Energy Explained: Theory, Design and Application*, John Wiley and Sons, 2010, p. 146;

[4] Menet, J. L., Bourabaa, N., *Increase in the Savonius Rotors Efficiency via a Parametric Investigation*, 2004 European Wind Energy Conference & Exhibition, 22-25 November, London, UK;

[5] Altan, B., D., Atilgan, M., *An Experimental and Numerical Study on the Improvement of the Performance of Savonius Wind Rotor*, Energy Conversion and Management, Vol. 49, Issue 12, December 2008, pp. 3425-3432;

[6] Nakajima, M., Ilo, Shouichiro, Ikeda, T., *Performance of Double-step Savonius Rotor for Environmentally Friendly Hydraulic Turbine*, Journal of Fluid Science and Technology, Vol. 3, No. 3, 2008, pp. 410-419;

[7] Saha, U., K., Rajkumar, M., J., *On the Performance Analysis of a Savonius Rotor with Twisted Blades*, Renewable Energy 31 (2006), pp. 1776-1788;

[8] Dominy, R., Lunt, P., Bickerdyke, A., Dominy, J., *Self-Strating Capability of a Darrieus Turbine*, JPE340©IMechE 2007, Proc. IMechE Vol. 221 Part A: J. Power and Energy;

[9] Gupta, R., Das, R., Sharma, K. K., *Experimental Study of a Savonius-Darrieus Wind Machine*, Proceedings of the International Conference on Renewable Energy for Developing Countries-2006;

[10] Bradshaw, P., *Experimental Fluid Mechanics*, Cambridge University Press, 1964;

[11] TorqueTrak Revolution – Torque and Power Monitoring System, User's Guide, Binsfeld Engineering Incorporated, MacFarlane Rd., Maple City, MI, USA;

[12] Di Carlo, F., *Torre eolica ad asse verticale spinta dalla sacca mobile*, Italian Patent N. RM2009A000326, Issued on June 25, 2009.